Inorganic Chemistry Communications 153 (2023) 110887

Contents lists available at ScienceDirect

Inorganic Chemistry Communications

journal homepage: www.elsevier.com/locate/inoche

Short communication

Phenytoin drug detection study through the $B_{24}N_{24}$ and $Al_{24}N_{24}$ nano-clusters in gas and solvent phase: DFT, TD-DFT, and thermodynamic study

Saade Abdalkareem Jasim [a], Andrés Alexis Ramírez-Coronel [b,c,d,e], Ameer A. Alameri [f], I.B. Sapaev [g,h], Yasser Fakri Mustafa [i], Abduladheem Turki Jalil [j,*], Qutaiba A. Qasim [k], Munther Abosaooda [l]

[a] Medical Laboratory Techniques Department, Al-maarif University College, Al-anbar-Ramadi, Iraq
[b] Catholic University of Cuenca, Azogues campus, Ecuador
[c] University of Palermo, Buenos Aires, Argentina
[d] National University of Education, Azogues, Ecuador
[e] CES University, Medellin, Colombia
[f] Department of Chemistry, College of Science, University of Babylon, Babylon, Iraq
[g] Tashkent Institute of Irrigation and Agricultural Mechanization Engineers, National Research University, Tashkent, Uzbekistan
[h] Akfa University, Tashkent, Uzbekistan
[i] Department of Pharmaceutical Chemistry, College of Pharmacy, University of Mosul, Mosul 41001, Iraq
[j] Medical Laboratories Techniques Department, Al-Mustaqbal University College, Babylon, Hilla 51001, Iraq
[k] College of Pharmacy, Al-Ayen University, Thi-Qar, Iraq
[l] College of Pharmacy, The Islamic University, 54001 Najaf, Iraq

ARTICLE INFO

Keywords:
Phenytoin
Boron nitride and aluminum nitride nano-clusters
Detection
Density functional theory

ABSTRACT

Chemical sensors could pioneer great utilities in point-of-care diagnostic medical devices. Therefore, the interaction of the $B_{24}N_{24}$ and $Al_{24}N_{24}$ nano-clusters with phenytoin was theoretically studied to explore a potential chemical sensor. All calculations were performed using the B3LYP-D method in the gas and solution phases. The absorption energies were −12.54 and −35.36 kcal mol^{-1} for $B_{24}N_{24}$ and $Al_{24}N_{24}$, in the most stable orientations, respectively. Thermodynamic investigations were shown the interaction of PHT with the nano-clusters is spontaneous and exothermic. Electrical conductivity after the adsorption process was changed to −23.94 % and −6.81 % in the $B_{24}N_{24}$ and $Al_{24}N_{24}$, respectively. Thus, it is clear that the $B_{24}N_{24}$ nano-cluster demonstrated a significant alteration in the electrical conductivity, and these changes could be considered the signal for the detection of PHT. Further, the $B_{24}N_{24}$ nano-cluster had a practical short recovery time of 1.52×10^{-5} s. Furthermore, solvent calculations indicated that the nano-clusters also could be used in biological samples. UV–vis calculation showed after the interaction of PHT with the $B_{24}N_{24}$ spectrum shifted significantly to the higher wavelength region (red shift). The concentration calculations showed a concentration-independent sensor response in the $B_{24}N_{24}$ nano-cluster. Thus, it can be concluded that the $B_{24}N_{24}$ nano-cluster is an appropriate candidate for PHT detection and this nano-cluster can be used in sensor devices.

1. Introduction

Phenytoin (PHT) is widely utilized to treat partial and generalized seizures [1]. PHT tends to attach to the main albumin as a plasma protein. It also exhibits a metabolism of concentration-dependent in the therapeutic range in cerebrospinal fluid, which corresponds to the plasma unbound concentration [2]. Further, there is a relation between the plasma unbound level of PTH and its toxicity [3]. However, despite its practical applications, some side effects and toxicities limit its clinical application. Swollen or sore gums, feeling unsteady, nervous, shaky, sleepy, dizzy, and headaches are potentially relevant problems [4]. Therefore, to prevent its adverse effect, it is critical to detect the

* Corresponding author.
E-mail address: abedalazeem799@gmail.com (A. Turki Jalil).

https://doi.org/10.1016/j.inoche.2023.110887
Received 21 February 2023; Received in revised form 28 April 2023; Accepted 26 May 2023
Available online 27 May 2023
1387-7003/

presence of PHT in human bodies; consequently, its administration can be careful.

Several studies have studied detection methods for PHT through high-performance liquid chromatography [5], gas chromatography-thermionic specific detection [6], capillary electrophoresis [7], and gas chromatography-mass spectrometry [8]. These techniques require expensive equipment, materials, and expert staff; also, they are time-consuming. So emerging rapid and reliable methods are highly demanded in these fields. Recently chemical sensors have attracted increasing attention because of facile fabrication, highly selective, highly sensitive, fast, and cost-effective application, portable platform, and recovery facilities [9–11]. Therefore, it is worth mentioning that chemical sensors have certainly had a very positive impact on the expansion of point-of-care strategies that can be easily adapted to real-world applications [12–14]. Nanomaterials play a significant role in this development. They take advantage of unique features such as high specific surface area, tunable structural and chemical properties, also enhanced diffusivity [15–22].

Several works have reported the excellent performance of aluminum nitride (AlN) and boron nitride (BN) nano-clusters as chemical sensors [23–28]. These nano-structured sensors profit from the benefits of groups III–V compounds in the Periodic Table, so their chemical bonding and structure attract great focus [15,29,30]. They have indicated appropriate performances due to their high oxidation resistance, high conductivity [31,32], chemical and thermal stability [33,34], and wide band gap [35]. Computational methods significantly help the experimentalist to understand different compounds' behavior [36–43].

Therefore, in this work, the detection properties of $Al_{24}N_{24}$ and $B_{24}N_{24}$ nano-clusters have been systematically evaluated through a density functional theory (DFT) study for PHT, extensively administrated for epilepsy treatment and other chronic diseases. Thus the study could pave the way for these nanostructures applications as suitable sensor candidates for PHT detection.

2. Computational method

Computations were conducted by the GAMESS software [44]. $B_{24}N_{24}$ and $Al_{24}N_{24}$ nano-clusters and their complexes were studied throughout the B3LYP-D technique and 6-31G(d) basis set [45–48]. Preceding studies reported the method as a dependable procedure because of its locating of weak interactions in the complexes [49,50]. Adsorption energies (E_{ad}) of PHT on the adsorbents' surface were calculated by applying the following equation:

E_{ad} = E(complex) – E(PHT) – E(adsorbent)(1).

where E(complex) refers to the total energy of PHT-interacted nanostructures. E(PHT) and E(adsorbent) are the total energy of lone PHT and nanostructures. Thermodynamic values (Gibbs free energy (ΔG), entropy (ΔS), and enthalpy (ΔH)) were also calculated to check the reliability of the optimized structure. The HOMO and LUMO, energy gap (Eg), and energy gap variation (ΔEg) were considered to compare the sensitivities. After the optimization, the time-dependent DFT approach (TD-DFT) from the ground state at B3LYP-D/6-31G(d) level was employed to obtain excited states to accomplish the UV–vis spectrum. Moreover, the influence of the solvent phase on the interaction of PHT with AlN and BN nanoclusters has been investigated using the polarizable continuum model (PCM) method at the B3LYP-D/6-31G(d) level [51]. The stability of pure nano-structures and PHT-interacted complexes in water was evaluated using solvent energy (ΔE_{solv}),

$\Delta E_{solv} = E_{solv}$ - E_{gas}(2).

E_{solv} is the compound's total energy in the solution phase, and E_{gas} is the total energy of the compound in the gaseous status. The same theory level was applied to compute the density of states (DOS), molecular electrostatic potential (MEP), and all energy computations. For providing the DOS plots GaussSam software was used, and for MEP plots GaussView software was utilized.

3. Results and discussion

3.1. PHT adsorption on $B_{24}N_{24}$ nano-cluster

Fig. 1 demonstrates the optimized structure and MEP plot of the PHT molecule. The MEP plot of PHT shows remarkable negative charges on its O atoms (red-colored) can interact with the electron-withdrawing sites in the nano-cluster. Fig. 2 demonstrates the optimized structure of the $B_{24}N_{24}$ nano-cluster and PHT/$B_{24}N_{24}$ complex. The most stable structure of the nano-cluster, as it can be seen, consists of eight-membered (8 M), six-membered (6 M), and four-membered (4 M) rings. The structural evaluation indicates that the bond length of B-N bonds in 8 M−6 M, 8 M−4 M, and 6 M−4 M mutual bonds at the structure were calculated at 1.42, 1.47, and 1.49 Å, respectively, which confirms previous findings [52,53]. Different PHT orientations were examined to investigate the best $B_{24}N_{24}$ nano-cluster interaction locations. Following the complex relaxation study, the two sites of O atoms of PHT, named states A and B, were selected (Fig. 2) as the two main orientations of PHT for interaction with the B atom of nano-cluster rendering to the E_{ad} values. These values for PHT adsorption were −12.54 and −3.61 kcal mol^{-1} in states A and B (Table 1). Hoseininezhad-Namin et al. calculated the adsorption energies of $Zn_{12}O_{12}$, $Mg_{12}O_{12}$, and Be12O12 nanoclusters at −60.17, −45.57, and –32.75 kcal mol^{-1}, respectively [54]. In addition to the 6-31G(d) basis set, we used the 6-311G(d, p) basis set. The result indicated another basis set has no significant influence on the results. The equilibrium distances between PHT and the nano-structure are 1.61 and 2.60 Å, respectively. Therefore, because of the higher adsorption energy and short equilibrium distance, interacted complex in state A is more stable. The result indicated another basis set has no significant influence on the results. The natural bond orbital (NBO) charge transfers from the PHT to the $B_{24}N_{24}$ in states A and B were investigated at 0.179 and 0.089 e, respectively. Positive values of NBO charge transfers illustrated that the charge transferred from PHT to $B_{24}N_{24}$ nanocluster.

3.2. PHT adsorption on $Al_{24}N_{24}$ nano-cluster

To investigate the effect of another nano-cluster, the adsorption properties of the Al24N24 nano-cluster with PHT were investigated. The $Al_{24}N_{24}$ nano-cluster is shown in Fig. 3. The bond length of B-N bonds in 8 M−6 M, 8 M−4 M, and 6 M−4 M mutual bonds at the structure were calculated at 1.78, 1.83, and 1.86 Å, respectively, which confirms other studies in this field [55,56]. $Al_{24}N_{24}$ nano-cluster with different orientations toward the PHT drug were examined to identify the optimized interaction sites. Similar to the adsorption on the $B_{24}N_{24}$ nano-cluster, PHT interacted appropriately with $Al_{24}N_{24}$ nano-cluster by its O atoms (Fig. 3). Considering the E_{ad} values of the most stable complexes, −35.36 and –32.76 kcal mol^{-1} for states A and B (see Table1), confirm these adsorptions are around 181 % and 807 % stronger than PHT/$B_{24}N_{24}$ complex. The equilibrium distances after the interaction were calculated at 1.61 and 2.60 Å for states A and B, respectively.

The dipole moment (DM), which varies following adsorption, is a vital indicator of the charge distribution throughout that process. Table 1 lists the DM values of PHT, $B_{24}N_{24}$, and $Al_{24}N_{24}$, as well as their most stable configurations. The $B_{24}N_{24}$ and $Al_{24}N_{24}$ nano-structures computed DM were 0.00 and 0.01, respectively. The DM of the nano-structure was considerably elevated to 9.19 and 6.52 Debye in their most stable state after PHT adsorption. The high polarization degree of the PHT interacting complexes, which results in polar interactions between PHT and nano-structures, causes the rise in DM values following adsorption.

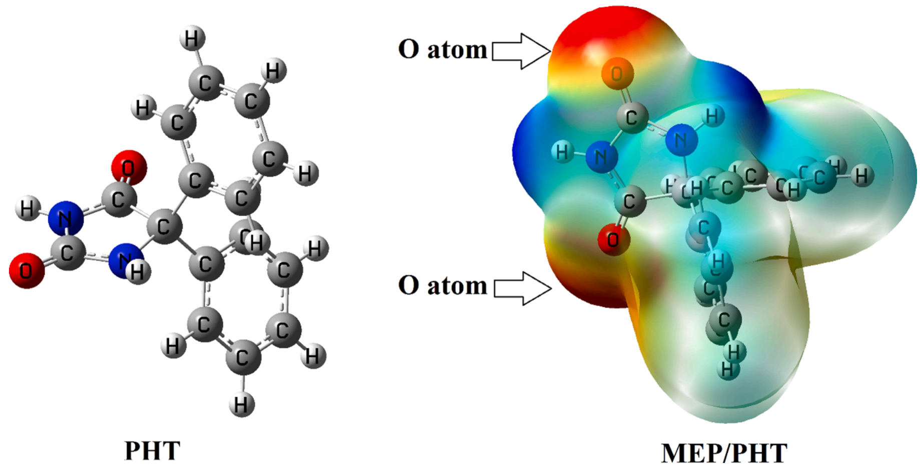

Fig. 1. Optimized structures and MEP plots of PHT.

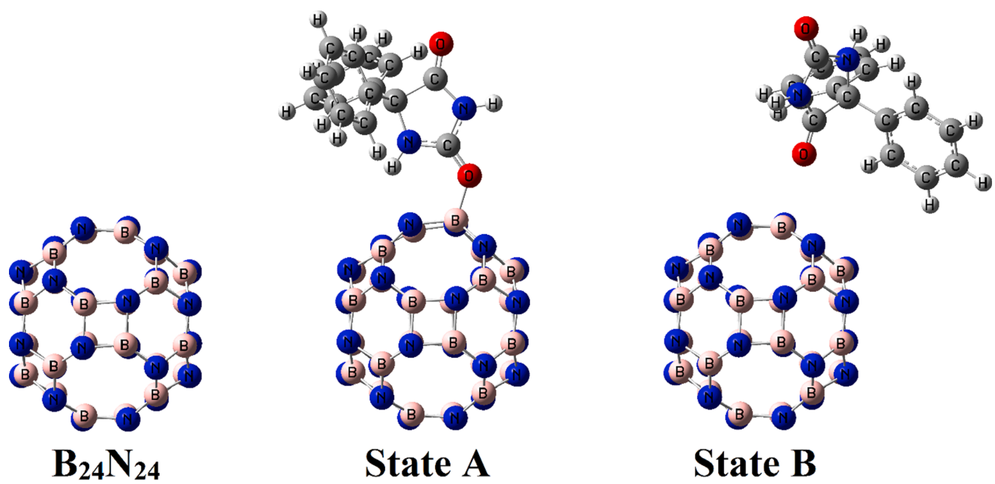

Fig. 2. Optimized structure of $B_{24}N_{24}$ and interaction of PHT molecule with $B_{24}N_{24}$ nano-cluster.

Table 1
Calculated adsorption energy (E_{ad}/kcal mol^{-1}), bond distance between PHT and nanocluster (D/Å), HOMO energies ($E_{(HOMO)}$/eV), LUMO energies ($E_{(LUMO)}$/eV), energy gap (E_g/eV), **%**ΔE_g change in electrical conductivity after the PHT adsorption, dipole moment (DM, Debye), enthalpy (ΔH/kJ mol^{-1}), Gibbs free energy (ΔG/kJ mol^{-1}) and entropy (ΔS/kJ K^{-1} mol^{-1}), in gas phase.

Name	E_{ad}	D	$E_{(HOMO)}$	$E_{(LUMO)}$	E_g	%ΔE_g	DM	ΔH	ΔG	ΔS
PHT	–	–	−6.66	−0.69	5.97	–	2.69	–	–	–
$B_{24}N_{24}$	–	–	−7.41	−0.93	6.48	–	0.00	–	–	–
$B_{24}N_{24}$ (State A)	−12.54	1.61	−6.67	−1.74	4.93	−23.94	9.19	−11.29	−4.25	−0.024
$B_{24}N_{24}$ (State B)	−3.61	2.60	−6.63	−0.94	5.69	−12.19	2.44	−2.72	3.68	−0.021
$Al_{24}N_{24}$	–	–	−6.48	−2.39	4.09	–	0.01	–	–	–
$Al_{24}N_{24}$ (State A)	−35.36	1.92	−5.95	−2.14	3.81	−6.81	6.52	−34.16	−21.69	−0.042
$Al_{24}N_{24}$ (State B)	−32.76	1.94	−6.01	−2.13	3.87	−5.38	7.76	−31.19	−19.39	−0.040

3.3. Thermodynamic analysis

The thermodynamic parameters at 298.15 K were investigated to check the optimized structures' reliability. Table 1 demonstrates the adsorption process's ΔG, ΔH, and ΔS values. The ΔH (ΔG) values for the $B_{24}N_{24}$ nano-cluster were obtained at −11.29 (−4.25) and −2.72 (3.68) kcal mol^{-1} for states A and B, respectively. These values corroborated that the adsorption of PHT from state A is stronger since the ΔH value was indicated to be more negative in state A. The ΔH and ΔG values in the $Al_{24}N_{24}$ nano-cluster, similar to the $B_{24}N_{24}$, indicated negative values in the most stable complexes. Thus, negative values indicated interaction of PHT with $B_{24}N_{24}$ and $Al_{24}N_{24}$ nano-clusters is exothermic and spontaneous. The calculated E_{ad} is more negative compared with the ΔG, indicating ΔS reduction. Furthermore, the ΔH values showed that the adsorption of PHT with $Al_{24}N_{24}$ was stronger than in the $B_{24}N_{24}$, which confirms the E_{ad} values.

3.4. Electrical properties of nano-clusters throughout the adsorption

The species' HOMO and LUMO energy levels were computed to evaluate the nano-clusters and the adsorption performances (see Table 1). The HUMO and LUMO energy levels of $B_{24}N_{24}$ are −7.41 and −0.93 eV, respectively. In the $Al_{24}N_{24}$, these values are calculated at −7.41 and −2.51 eV. Abdalkareem Jasim et al. calculated the HOMO

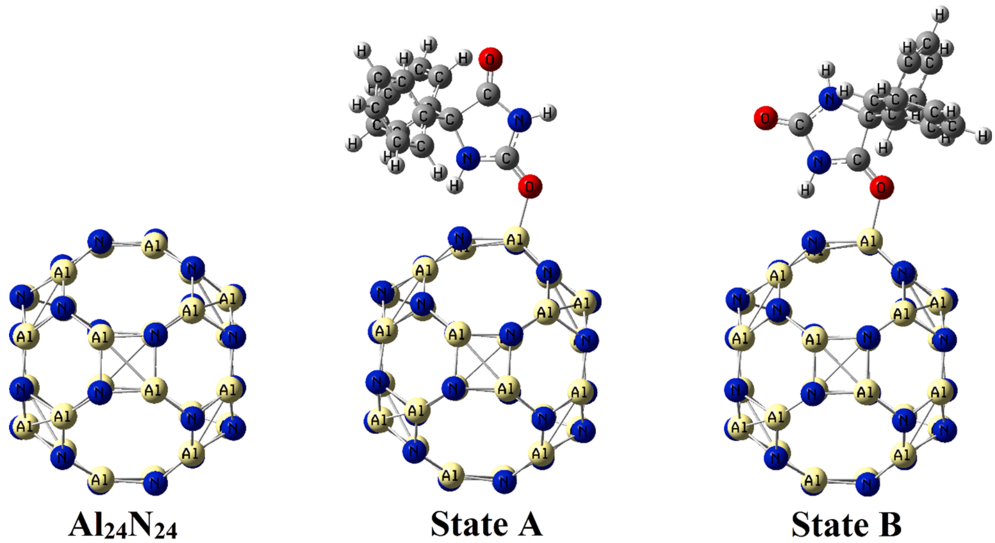

Fig. 3. Optimized structure of $Al_{24}N_{24}$ and interaction of PHT molecule with $Al_{24}N_{24}$ nano-cluster.

and LUMO of $B_{24}N_{24}$ at −7.15 and −2.30 eV, respectively, and the $Al_{24}N_{24}$ nano-cluster was calculated at −6.50 and −2.30 eV, which confirmed obtained results [15].

On the other hand, PHT adsorption on nano-clusters causes significant changes in HUMO and LUMO energy levels and, consequently, their differences. The energy gap (E_g) is a good indicator of a sensor's electrical conductivity (sensitivity) for a specific molecule and is calculated by the (LUMO-HOMO) energy levels. Equation 3 described the relationship between the electrical conductivity (σ) and E_g [44]:

$\sigma \propto \exp(-E_g/2k_BT)$(3).

In which T and K_B are the temperatures and Boltzmann constant, respectively. According to equation 3, variations in the E_g cause changes in electrical conductivity. The energy gap and its variation are given in Table 1. PHT adsorption causes –23.94 % and −6.81 % variations in the E_g of the $B_{24}N_{24}$ and $Al_{22}N_{24}$ nano-clusters, respectively. The results show higher sensitivity of $B_{24}N_{24}$ nano-cluster for PHT adsorption and its detection.

As shown in Fig. 4, the density of states (DOS) diagram, in conjunction with the molecular electrostatic potential plot (MEP), illustrates more details of PHT molecules' adsorption on nano-structures in the most stable complexes (states A). The interaction characteristics of

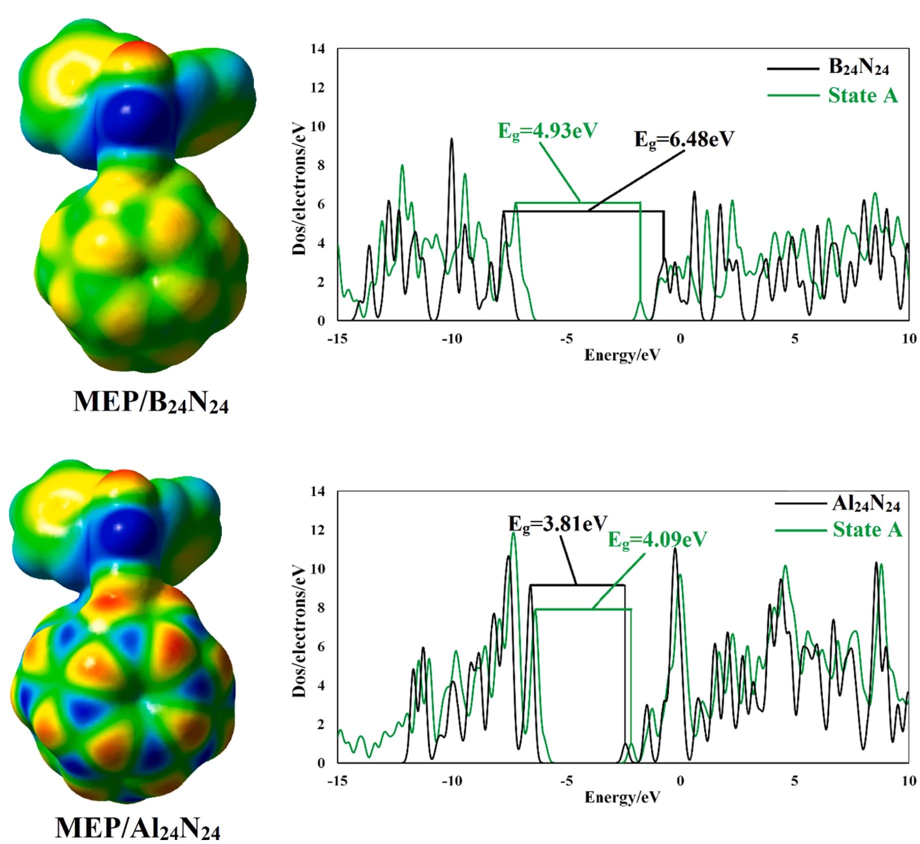

Fig. 4. MEP and DOS plots of PHT/$B_{24}N_{24}$ (state A) and PHT/$Al_{24}N_{24}$ (state A).

PHT adsorption on $B_{24}N_{24}$ and $Al_{24}N_{24}$ are described in the DOS diagrams. It can be seen that PHT adsorption changes the DOS spectrum and HUMO and LUMO energy levels in the nano-structures. The adsorption changes energy levels in all $B_{24}N_{24}$ and $Al_{24}N_{24}$ nano-structures, confirming the values shown in Table 1. Furthermore, the movement of the location of the peaks demonstrates that interaction between the PHT molecules and nano-structure is because of electron transfer between them.

In addition, compared with the bare nano-structures, MEP plots of the most stable complexes in Fig. 4 show remarkable changes after PHT adsorption in their electrostatic potential. The plots indicate that the PHT drug in the complexes is more positive (blue color), and the nano-structures are more negative (red color). Therefore, these findings confirm charge transferring from PHT molecules to the nano-clusters, which corroborates the outcome of values charge transfers.

3.5. Solution phase influence on PHT drug interaction with the nano-structures

Water was chosen as a similar medium to assess the PHT interaction with the nano-structures in the body's physiological fluid. The pure PHT, nano-clusters, and most stable complexes were optimized by applying the B3LYP-D/6-31G(d) level of theory. The calculated solvation energies (E_{sol}) from Eq. (2) were −8.58 and −27.19 kcal mol^{-1} for pure $B_{24}N_{24}$ and $Al_{24}N_{24}$ nano-structures, respectively; these negative values show that they are soluble in the aqueous phase [57]. The matching values for PHT interacted complexes were −17.09 and –33.70 kcal mol^{-1} (Table 2), respectively. The more negative solvation energies display superior solubility and stability, representing all nanostructure's possible applications for PHT well detection in the water phase.

Furthermore, the adsorption energies of PHT on the nano-structures in the water are given in the same Table. The values are −12.54 and −35.36 kcal mol^{-1} for $B_{24}N_{24}$ and $Al_{24}N_{24}$. Therefore, adsorption energies indicated no significant alteration compared with the gas phase. In addition, comparing the DM values of PHT-interacted nanostructures in the gaseous and aqueous phases (Tables 1 and 2) reveals higher values in the water phase, which indicates that nano-structures have more conductivity and reactivity toward the PHT molecules in this phase. Also, the %ΔE_g variations in the water phase represent the developed sensitivity of $B_{24}N_{24}$ nano-structure for PHT detection, which confirms the similar result in the gas phase.

3.6. UV–Vis spectra

UV–vis spectra of pure and PHT-interacted nanostructures were investigated by applying TD-DFT calculations. The highest oscillator strengths (*f*) for the current studied system are presented in Table 3. The maximum absorption wavelength (λ_{max}) in the spectra of $B_{24}N_{24}$ and $Al_{24}N_{24}$ is located at 218 and 350 nm, respectively. PHT adsorption causes replacement of the λ_{max} towards 263 and 381 nm in PHT/$B_{24}N_{24}$ and PHT/$Al_{24}N_{24}$ complexes, respectively. Therefore, after interaction with PHT molecules, the λ_{max} shifted to the higher wavelengths (red-shift) with lower energies. More significant movements to the other wavelengths are attributed to the adsorbent's increased conductivity due to the changes in orbitals energy after PHT adsorption [58]. The results explicitly confirm the energy gap variation in Table 1, and this movement to the higher wavelength region (red-shift) is significant for $B_{24}N_{24}$. The Table also presents the main transition contributions of the PHT molecule interaction with the nano-clusters.

Table 3
Maximum absorption wavelength (λ_{max}), oscillator strength (f), and main contributions of the pure and interacted nano-structures in their UV spectra.

Molecule	λ_{max} (nm)	*f*	Major contribution
$B_{24}N_{24}$	218	0.00001	H-1 → LUMO (24 %), HOMO → LUMO (27 %), HOMO → L + 1 (20 %)
PHT/ $B_{24}N_{24}$	263	0.0267	H-5 → LUMO (44 %), H-4 → LUMO (18 %), H-6 → LUMO (18 %)
$Al_{24}N_{24}$	350	0.0001	H-2 → LUMO (95 %)
PHT/ $Al_{24}N_{24}$	381	0.0006	HOMO → LUMO (96 %)

3.7. Recovery time of nano-structures

As suitable interaction is essential for a detector, its recovery time is another critical factor for its development. From this point of view, strong adsorption may lead to a considerable desorption time, which is not practical for detection. Experimentally the recovery time is investigated under UV light exposure or heating to high temperatures. The recovery time can be calculated through the following question of transition theory:

$\tau = \upsilon-^{1} \exp(-E_{ad} / kT)(4).$

where T, k, and ν_0 are temperature, Boltzmann's constant, and try frequency, respectively. Here, recovery time was calculated by considering the frequency of 10^{14} s^{-1} ($\nu \sim 10^{14}$ s^{-1}) at room temperature (298.15 K). The needed time for desorption of the PHT molecules from the PHT/$B_{24}N_{24}$ and PHT/$Al_{24}N_{24}$ nano-clusters was about 1.52×10^{-5} and 7.86×10^{11} s. Findings show that the recovery time of the $B_{24}N_{24}$ is short and feasible, whereas the $Al_{24}N_{24}$ nano-structure suffers from a long recovery time, and PHT adsorption is almost irreversible on them. Therefore, pristine $B_{24}N_{24}$ nano-structure comprises a supreme recovery time and is a suitable detector of PHT molecules.

3.8. Effect of concentration

For the investigation of concentration effects, different numbers of PHT drugs were adsorbed on the BN nano-cluster (Fig. 5). The E_{ad} of PHT on the $B_{24}N_{24}$ nano-cluster with 2, 3, and 4 molecules was calculated at −11.57, −10.45, and −9.45 Kcal.mol^{-1}, respectively, which was −12.54 Kcal.mol^{-1} for one molecule of it (Table 4). Due to steric repulsions between the molecules with increasing the concentration of PHT, the E_{ad} indicates less negative. The increase in concentration has a lesser influence on electronic properties, with an alteration of E_g in the confine of 4.21–4.74 eV, which was 4.93 eV considering one PHT molecule. Considering the %ΔE_g after adsorption of more than one number of PHT molecule on the nano-cluster, it is obvious that the most considerable variation happens after the one-molecule interaction and the interaction of more than one molecule has a more negligible effect.

Table 2
Calculated solvent energy (ΔE_{solv}/kcal mol^{-1}), adsorption energy (E_{ad}/ kcal mol^{-1}), bond distance between PHT and nanocluster (D/Å), HOMO energies ($E_{(HOMO)}$/eV), LUMO energies ($E_{(LUMO)}$/eV), energy gap (E_g/eV), %ΔE_g change in electrical conductivity after the PHT adsorption, and dipole moment (DM, Debye), in solvent phase.

Name	ΔE_{solv}	E_{ad}	D	$E_{(HOMO)}$	$E_{(LUMO)}$	E_g	%ΔE_g	DM
PHT	−8.82	–		−6.70	−0.78	5.92	–	3.35
$B_{24}N_{24}$	−8.58	–	–	−7.27	−0.73	6.54	–	0.02
PHT/$B_{24}N_{24}$	−17.09	−12.54	1.58	−6.78	−1.41	5.36	−18.04	11.20
$Al_{24}N_{24}$	−27.19	–	–	−6.47	−2.23	4.24	–	0.03
PHT/$Al_{24}N_{24}$	−33.70	−35.36	1.91	−6.13	−2.13	4.00	−5.66	8.06

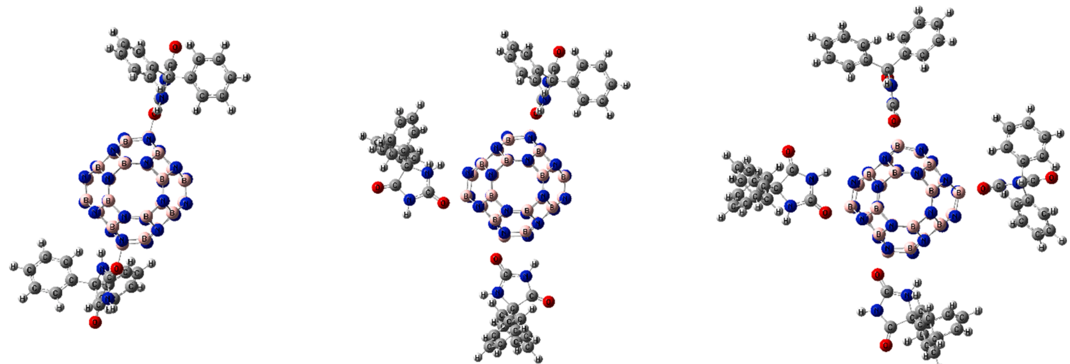

(A) (B) (C)

Fig. 5. Optimized orientations of 2(A), 3(B), and 4(C) PHT molecules toward the $B_{24}N_{24}$ nanocluster.

Table 4
Calculated adsorption energy (Ead), HOMO (E_{HOMO}), and LUMO (E_{LUMO}) energies, energy gap (E_g), %ΔEg change in electrical conductivity after the PHT adsorption on the $B_{24}N_{24}$ nanocluster.

Name	E_{ad} (kcal mol^{-1})	E_{HOMO} (eV)	E_{LUMO} (eV)	E_g (eV)	%ΔE_g
$B_{24}N_{24}$	–	−7.41	−0.93	6.48	–
2-PHT	−11.57	−6.24	−1.50	4.74	−26.85
3-PHT	−10.45	−5.70	−1.33	4.37	−32.56
4-PHT	−9.25	−5.37	−1.16	4.21	−35.03

Thus, these values indicated a concentration-independent sensor response.

4. Conclusions

Current work investigated the interactions of $B_{24}N_{24}$ and $Al_{24}N_{24}$ nano-structures with PHT drug using DFT calculations to evaluate their detecting potential. The computed E_{ad} was −12.54 and −35.36 kcal mol^{-1} for PHT adsorption on the nano-structures in their most stable configuration, respectively. The energy gap variations and DOS plots confirmed $B_{24}N_{24}$ nano-structure has higher sensitivity toward the PHT drug. On the other hand, recovery time calculations revealed $B_{24}N_{24}$ nano-structures has a short recovery time of 1.52×10^{-5} s for desorption of the adsorbed PHT. The solvent energy values showed that the pure and PHT interacted nano-structures are stable in the water solution and can be applied as aqueous phase detectors. Consequently, these outcomes firmed that the $B_{24}N_{24}$ nano-structure can be a promising sensor for PHT detection.

Declaration of Competing Interest

The authors declare that they have no known competing financial interests or personal relationships that could have appeared to influence the work reported in this paper.

Data availability

No data was used for the research described in the article.

References

[1] Y. Yaari, M.E. Selzer, J.H. Pincus, Phenytoin: Mechanisms of its anticonvulsant action, Ann. Neurol. 20 (1986) 171–184.
[2] S. Botros, N.A. Khalil, B.H. Naguib, Y. El-Dash, Synthesis and anticonvulsant activity of new phenytoin derivatives, Eur. J. Med. Chem. 60 (2013) 57–63.
[3] G. Peterson, S. McLean, S. Aldous, R. Von Witt, K. Millingen, Plasma protein binding of phenytoin in 100 epileptic patients, Br. J. Clin. Pharmacol. 14 (1982) 298–300.
[4] N. Scheinfeld, Phenytoin in cutaneous medicine: Its uses, mechanisms and side effects, Dermatol. Online J. 9 (2003) 83–106.
[5] Z. Mei, J. Williams, Simultaneous determination of phenytoin and carbamazepine in human hair by high-performance liquid chromatography, Ther. Drug Monit. 19 (1997) 92–94.
[6] M.E.C. Queiroz, S.M. Silva, D. Carvalho, F.M. Lancas, Determination of lamotrigine simultaneously with carbamazepine, carbamazepine epoxide, phenytoin, phenobarbital, and primidone in human plasma by SPME-GC-TSD, J. Chromatogr. Sci. 40 (4) (2002) 219–223.
[7] Y. Kataoka, K. Makino, R. Oishi, Capillary electrophoresis for therapeutic drug monitoring of antiepileptics, Electrophoresis 19 (16-17) (1998) 2856–2860.
[8] D.J. Speed, S.J. Dickson, E.R. Cairns, N.D. Kim, Analysis of six anticonvulsant drugs using solid-phase extraction, deuterated internal standards, and gas chromatography-mass spectrometry, J. Anal. Toxicol. 24 (2000) 685–690.
[9] J.F. Olorunyomi, S.T. Geh, R.A. Caruso, C.M. Doherty, Metal-organic frameworks for chemical sensing devices, Mater. horizons 8 (9) (2021) 2387–2419.
[10] V. Montes-García, M.A. Squillaci, M. Diez-Castellnou, Q.K. Ong, F. Stellacci, P. Samorì, Chemical sensing with Au and Ag nanoparticles, Chem. Soc. Rev. 50 (2) (2021) 1269–1304.
[11] Z. Zhang, P. Ma, R. Ahmed, J. Wang, D. Akin, F. Soto, B.-F. Liu, P. Li, U. Demirci, Advanced Point-of-Care Testing Technologies for Human Acute Respiratory Virus Detection, Adv. Mater. 34 (1) (2022) 2103646.
[12] M.R. Karim, M.M. Alam, M.O. Aijaz, A.M. Asiri, F.S. Almubaddel, M.M. Rahman, The fabrication of a chemical sensor with PANI-TiO2 nanocomposites, RSC Adv. 10 (2020) 12224–12233.
[13] R. Mandal, A. Baranwal, A. Srivastava, P. Chandra, Evolving trends in bio/chemical sensor fabrication incorporating bimetallic nanoparticles, Biosens. Bioelectron. 117 (2018) 546–561.
[14] Y. Cui, Intelligent Management of Clinical Application of Antibacterial Drugs Based on Improved Single-Shot Detector Algorithm, in: INDIAN JOURNAL OF PHARMACEUTICAL SCIENCES, INDIAN PHARMACEUTICAL ASSOC KALINA, SANTA CRUZ EAST, MUMBAI, 00000, INDIA, 2021, pp. 37-37.
[15] S. Abdalkareem Jasim, F.H. Alsultany, M.Z. Mahmoud, D. Olegovich Bokov, W. Suksatan, Investigations of chemical sensing properties of Al24N24, B24N24, and B24P24 nanoclusters toward carbamazepine: A DFT study, Inorg. Chem. Commun. 142 (2022).
[16] L. Lu, J. Dong, Y. Liu, Y. Qian, G. Zhang, W. Zhou, A. Zhao, G. Ji, H. Xu, New insights into natural products that target the gut microbiota: Effects on the prevention and treatment of colorectal cancer, Front. Pharmacol. 13 (2022).
[17] C. Zhang, J. Li, M. Xiao, D. Wang, Y. Qu, L. Zou, C. Zheng, J. Zhang, Oral colon-targeted mucoadhesive micelles with enzyme-responsive controlled release of curcumin for ulcerative colitis therapy, Chin. Chem. Lett. 33 (2022) 4924–4929.
[18] K.Q. Zhang, Q.F. Deng, J. Luo, C.L. Gong, Z.G. Chen, W. Zhong, S.Q. Hu, H. F. Wang, Multifunctional ag(i)/caaa-amidphos complex-catalyzed asymmetric [3 + 2] cycloaddition of α-substituted acrylamides, ACS Catal. 11 (2021) 5100–5107.
[19] X. Feng, L. Jiang, D. Li, S. Tian, X. Zhu, H. Wang, C. He, K. Li, Progress and key challenges in catalytic combustion of lean methane, J. Energy Chem. 75 (2022) 173–215.
[20] H. Luo, Y. Lou, K. He, Z. Jiang, Coupling in-situ synchrotron X-ray radiography and FT-IR spectroscopy reveal thermally-induced subsurface microstructure evolution of solid propellants, Combust. Flame 249 (2023) 112609.
[21] Z. Wang, L. Dai, J. Yao, T. Guo, D. Hrynsphan, S. Tatsiana, J. Chen, Improvement of Alcaligenes sp.TB performance by Fe-Pd/multi-walled carbon nanotubes: Enriched denitrification pathways and accelerated electron transport, Bioresour. Technol. 327 (2021).
[22] M. Qu, T. Liang, J. Hou, Z. Liu, E. Yang, X. Liu, Laboratory study and field application of amphiphilic molybdenum disulfide nanosheets for enhanced oil recovery, J. Pet. Sci. Eng. 208 (2022) 109695.
[23] R. Ghiasi, A. Valizadeh, Computational investigation of interaction of a cycloplatinated thiosemicarbazone as antitumor and antiparasitic agents with B12N12 nano-cage, Results Chem. 5 (2023) 100768.
[24] M. Shabani, R. Ghiasi, K. Zare, R. Fazaeli, Computational investigation of interaction between titanocene dichloride and nanoclusters (B12N12, B12P12, Al12N12and Al12P12), Main Group Chem. 20 (2021) 437–446.

[25] R. Ghiasi, R. Emami, M. Vasfi Sofiyani, Interaction between carboplatin with B12P12 and Al12P12 nano-clusters: A computational investigation, Phosphorus Sulfur Silicon Relat. Elem. 196 (8) (2021) 751–759.
[26] R. Ghiasi, M. Rahimi, Complex formation of titanocene dichloride anticancer and Al12N12 nano-cluster: A quantum chemical investigation of solvent, temperature and pressure effects, Main Group Chem. 20 (2021) 19–32.
[27] M. Shabani, R. Ghiasi, K. Zare, R. Fazaeli, The interaction between carboplatin anticancer drug and B12N12 nano-cluster: A computational investigation, Main Group Chem. 20 (3) (2021) 345–354.
[28] S. Mozhdeh, R. Ghiasi, K. Zare, R. Fazaeli, Quantum Chemical Study of Interaction between Titanocene Dichloride Anticancer Drug and Al12N12 Nano-Cluster, Russ. J. Inorg. Chem. 65 (2020) 1726–1734.
[29] Z. Mahdavifar, Prediction of unexpected B: N Pn structures: promising materials for non-linear optical devices and photocatalytic activities, Nanoscale Adv. 3 (2021) 2846–2861.
[30] M.S. Hoseininezhad-Namin, E. Rahimpour, S. Aysil Ozkan, P. Pargolghasemi, A. Jouyban, Sensing of carbamazepine by AlN and BN nanoclusters in gas and solvent phases: DFT and TD-DFT calculation, J. Mol. Liq. 353 (2022).
[31] E. Golipour-Chobar, F. Salimi, G. Ebrahimzadeh Rajaei, Boron nitride nanocluster as a carrier for lomustine anticancer drug delivery: DFT and thermodynamics studies, Monatsh. Chem. 151 (3) (2020) 309–318.
[32] R. Gholami, M. Solimannejad, Potential of B24N24 nanocluster for sensing and delivering aloe-emodin anticancer drug: A DFT study, J. Mol. Struct. 1270 (2022) 133968.
[33] FUZHANG Wang, M.N. Khan, IMTIAZ Ahmad, HIJAZ Ahmad, HANAA Abu-zinadah, YU.-MING. Chu, Numerical Solution Of Traveling Waves In Chemical Kinetics: Time-Fractional Fishers Equations, Fractals 30 (02) (2022).
[34] T.H. Zhao, Z.Y. He, Y.M. Chu, On some refinements for inequalities involving zero-balanced hypergeometric function, AIMS Math. 5 (2020) 6479–6495.
[35] M. Solimannejad, M. Noormohammadbeigi, Boron nitride nanotube (BNNT) as a sensor of hydroperoxyl radical (HO2): A DFT study, J. Iran. Chem. Soc. 14 (2) (2017) 471–476.
[36] R. Ghiasi, A. Valizadeh, Interaction of cisplatin anticancer drug with C20bowl: DFT investigation, Main Group Chem. 21 (1) (2022) 43–54.
[37] R. Ghiasi, M.V. Sofiyani, R. Emami, Computational investigation of interaction of titanocene dichloride anti-cancer drug with carbon nanotube in the presence of external electric field, Biointerface Res. Appl. Chem. 11 (2021) 12454–12461.
[38] R. Ghiasi, M. Rahimi, R. Ahmadi, QUANTUM-CHEMICAL INVESTIGATION OF THE COMPLEXATION OF TITANOCENE DICHLORIDE WITH C20 AND M +@C20 (M + = Li, Na, K) CAGES, J. Struct. Chem. 61 (2020) 1681–1690.
[39] W. Liu, C. Zhao, Y.u. Zhou, X. Xu, A. Rakkesh R, Modeling of Vapor-Liquid Equilibrium for Electrolyte Solutions Based on COSMO-RS Interaction, J. Chem. 2022 (2022) 1–13.
[40] L.-Q. Chen, Y. Zhao, From classical thermodynamics to phase-field method, Prog. Mater. Sci. 124 (2022) 100868.
[41] B. Fan, X. Zhao, Z. Liu, Y. Xiang, X. Zheng, Inter-component synergetic corrosion inhibition mechanism of Passiflora edulia Sims shell extract for mild steel in pickling solution: Experimental, DFT and reactive dynamics investigations, Sustain. Chem. Pharm. 29 (2022).
[42] H. Wang, C. Gong, Z. Zhou, Q. Zhou, Y. Liu, J. Luo, CHIRAL 1,2-DIAMINOCYCLOHEXANE-α-AMINO ACID-DERIVED AMIDPHOS/Ag(I)-CATALYZED DIVERGENT ENANTIOSELECTIVE 1,3-DIPOLAR CYCLOADDITION of AZOMETHINE YLIDES, Heterocycles 104 (2021) 123–139.
[43] D. Chen, Y. Li, X. Li, X. Hong, X. Fan, T. Savidge, Key difference between transition state stabilization and ground state destabilization: increasing atomic charge densities before or during enzyme-substrate binding, Chem. Sci. 13 (2022) 8193–8202.
[44] M.W. Schmidt, K.K. Baldridge, J.A. Boatz, S.T. Elbert, M.S. Gordon, J.H. Jensen, S. Koseki, N. Matsunaga, K.A. Nguyen, S. Su, T.L. Windus, M. Dupuis, J. A. Montgomery Jr., General atomic and molecular electronic structure system, J. Comput. Chem. 14 (1993) 1347–1363.
[45] A.D. Becke, Becke's three parameter hybrid method using the LYP correlation functional, J. Chem. Phys 98 (1993) 5648–5652.
[46] T.-H. Zhao, M.-K. Wang, W. Zhang, Y.-M. Chu, Quadratic transformation inequalities for Gaussian hypergeometric function, J. Inequal. Appl. 2018 (1) (2018).
[47] B. Civalleri, C.M. Zicovich-Wilson, L. Valenzano, P. Ugliengo, B3LYP augmented with an empirical dispersion term (B3LYP-D*) as applied to molecular crystals, Crystengcomm 10 (2008) 405–410.
[48] M.W. Wong, P.M.W. Gill, R.H. Nobes, L. Radom, 6–311G(MC)(d, p): A second-row analogue of the 6–311G(d, p) basis set. Calculated heats of formation for second-row hydrides, J. Phys. Chem. 92 (1988) 4875–4880.
[49] F. Nattagh, S. Hosseini, M.D. Esrafili, Effects of B and N doping/codoping on the adsorption behavior of C60 fullerene towards aspirin: A DFT investigation, J Mol. Liq. 342 (2021).
[50] P. Singla, M. Riyaz, S. Singhal, N. Goel, Theoretical study of adsorption of amino acids on graphene and BN sheet in gas and aqueous phase with empirical DFT dispersion correction, Phys. Chem. Chem. Phys. 18 (2016) 5597–5604.
[51] E. Chigo-Anota, A. Escobedo-Morales, H. Hernández-Cocoletzi, J.G. López Y López, Nitric oxide adsorption on non-stoichiometric boron nitride fullerene: Structural stability, physicochemistry and drug delivery perspectives, Phys E, 74 (2015) 538-543.
[52] Z. Rostami, M. Pashangpour, R. Moradi, DFT study on the chemical sensing properties of B24N24 nanocage toward formaldehyde, J. Mol. Graph. Model. 72 (2017) 129–135.
[53] M.K. Hazrati, Z. Javanshir, Z. Bagheri, B24N24 fullerene as a carrier for 5-fluoro-uracil anti-cancer drug delivery: DFT studies, J. Mol. Graph. Model. 77 (2017) 17–24.
[54] M.S. Hoseininezhad-Namin, Z. Javanshir, E. Rahimpour, A. Jouyban, Investigation on the potential application of some metal oxide nanoclusters in the detection of phenytoin in gas and solvent phases through density functional theory calculations, Inorg. Chem. Commun. 150 (2023) 110526.
[55] M.M.R. Nayini, H. Sayadian, N. Razavipour, M. Rezazade, Chemical-sensing of Amphetamine drug by inorganic AlN nano-cage: A DFT/TDDFT study, Inorg. Chem. Commun. 121 (2020).
[56] S. Sayhan, A. Kinal, Computational investigation and comparison of hydrogen storage properties of B24N24 and Al24N24 nanocages, Int. J. Hydrogen Energy 42 (2017) 14166–14180.
[57] A. Soltani, A. Sousaraei, M. Bezi Javan, M. Eskandari, H. Balakheyli, Electronic and optical properties of 5-AVA-functionalized BN nanoclusters: A DFT study, New J. Chem. 40 (8) (2016) 7018–7026.
[58] H. Sajid, S. Khan, K. Ayub, T. Mahmood, High selectivity of cyclic tetrapyrrole over tetrafuran and tetrathiophene toward toxic chemicals; A first-principles study, Microporous Mesoporous Mater. 299 (2020) 110126.